Nonlinear Laser Driven Donut Wakefields for Positron and Electron Acceleration

J. Vieira* and J. T. Mendonça†
GoLP/Instituto de Plasmas e Fusão Nuclear, Instituto Superior Técnico, Universidade de Lisboa, 1049-001 Lisboa, Portugal
(Received 5 February 2014; published 27 May 2014)

We show analytically and through three-dimensional particle-in-cell simulations that nonlinear wakefields driven by Laguerre-Gaussian laser pulses can lead to hollow electron self-injection and positron acceleration. We find that higher order lasers can drive donut shaped blowout wakefields with strong positron accelerating gradients comparable to those of a spherical bubble. Corresponding positron focusing forces can be more than an order of magnitude stronger than electron focusing forces in a spherical bubble. Required laser intensities and energies to reach the nonlinear donut shaped blowout are within state-of-the-art experimental conditions.

DOI: 10.1103/PhysRevLett.112.215001 PACS numbers: 52.38.Kd, 52.35.Mw, 52.65.Rr

Laser plasma interactions play a central role in several applications ranging from table-top laser wakefield accelerators (LWFA) [1,2] and light sources [3] to laser fusion [4]. So far, laser plasma research has been geared towards the use of drivers with Gaussian transverse profiles. Using these laser drivers in LWFA, for instance, lead to remarkable achievements [5]. Important LWFA experimental results have been reached in the strongly nonlinear bubble or blowout regime [6–8]. The blowout provides higher accelerating gradients ($\lesssim 1$ GeV/cm) and efficiencies in comparison to the linear regime. In addition, it also provides linear accelerating and transverse focusing forces, where electrons can accelerate with minimal emittance growth [9]. Thus, the nonlinear regime of LWFA has the potential to lead to a high quality electron source for science and applications.

Although ideally suited for electron trapping [10] and acceleration [11], the blowout is not adequate for positron acceleration. Instead of bringing positrons towards the axis, the transverse focusing force in the blowout regime defocuses positrons everywhere except in a narrow region where plasma electrons cross the axis at the back of the bubble. Several positron acceleration schemes were then proposed to optimize positron acceleration in plasmas. The nonlinear suck-in regime, for instance, provides positron accelerating and focusing fields similar to the linear or mildly nonlinear regime [12]. Hollow plasma channels [13,14] were also proposed for positron acceleration in the linear regime [15]. Despite these advances, studying new configurations for positron acceleration in the nonlinear regime is important and may impact a future plasma based linear collider.

There has been an increasing interest on the interaction between plasmas and lasers with orbital angular momentum (OAM). The production of these lasers, described by higher order Laguerre-Gaussian modes, is currently well understood [16]. Raman and Brillouin backscattering [17], and the inverse Faraday effect were then recently examined [18] using higher order lasers in plasmas. Linear wakefield excitation by lasers with OAM was also recently investigated [19]. Nevertheless, the use of these lasers to drive nonlinear wakefields for electron and positron acceleration is still unexplored.

In this work we demonstrate analytically and through 3D particle-in-cell (PIC) simulations in OSIRIS [20] that laser pulses with OAM can excite high-gradient positron focusing and accelerating wakefields in the nonlinear regime. We show that there are two limiting scenarios: at lower intensities, close to the onset of the blowout, the driver excites a donut bubble that can trap and accelerate hollow electron bunches, which can be relevant for applications [21]. At higher laser intensities, the inner electron sheath that surrounds the donut wakefield merges on axis. This results in strongly nonlinear wakefields that can focus and accelerate positrons. Moreover, the resulting focusing force can be more than an order of magnitude stronger than in pure ion channels.

To investigate wakefield excitation by lasers with OAM, we adopt the comoving frame variables, where $(x, y, \xi = z - ct, t)$, with (x, y) the transverse coordinates, and t and z the time and propagation distance. In addition, we use cylindrical coordinates where $r = \sqrt{x^2 + y^2}$ is the distance to the axis and where θ is the azimuthal angle. The normalized vector potential ($a_L = eA_L/m_e c$) of a laser with OAM at the focus is given by $a_L(r, \xi) = a_0 a_\parallel(\xi) a_r(r)$, where a_0 is the peak laser vector potential, $a_\parallel(\xi)$ is the longitudinal intensity profile normalized to a_0, and $a_r(r)$ is the transverse laser profile given by $a_r(r) = c_{l,p}(r/w_0)^{|l|} \exp(-r^2/w_0^2 + il\theta) L_p^{|l|}(2r^2/w_0^2)$, where w_0 is the spot size, L_p^l a Laguerre polynomial with radial index p and azimuthal index l, and where $c_{l,p}$ are normalizing factors. Unless explicitly stated, we normalize electric fields $\mathbf{E}$ to $m_e c^2 \omega_p/e$, magnetic fields $\mathbf{B}$ to

$m_e c\omega_p/e$, vector potentials $\mathbf{A}$ to $m_e c/e$, distances $\mathbf{x}$ to c/ω_p, and time t to ω_p. Here m_e and e are the electron mass and charge, ω_p the plasma frequency, and c the speed of light. Density is normalized to the background plasma density n_0 and velocity $\mathbf{v}$ to c.

Linear theory for wake excitation by lasers with OAM was derived in the limit where the laser central frequency (ω_0) respects $\omega_0/\omega_p \gg 1$. Corresponding accelerating (E_z) and focusing (W_r) wakefields acting on a relativistic particle are $E_z = -(1/4)\int_{-\infty}^{\xi} \sin(\xi-\xi')[\partial a_L^2(r,\xi')/\partial\xi]d\xi'$ [15,19,22], and $\partial W_r/\partial\xi = \partial E_z/\partial r$ with $W_r = E_r - B_\theta$, and where E_r and B_θ are the transverse electric and azimuthal magnetic fields. For a flattop laser pulse with $a_\parallel = \Theta(\xi) - \Theta(\xi-\lambda_p/2)$, where $\Theta(x)$ is the Heaviside step function, and $(l,p) = (1,0)$,

$$E_z = -\frac{a(r)^2}{2}\sin(\xi), \tag{1a}$$

$$W_r = \frac{a(r)^2}{r}\left(1 - \frac{2r^2}{{w_0}^2}\right)\cos(\xi), \tag{1b}$$

for $\xi > \lambda_p/2$. Equation (1a) shows that the amplitude of the wakefield is maximized in the region where $a_r^2(r)$ is maximum, i.e., in a donut shaped region around $r_m \simeq w_0/\sqrt{2}$. In addition, Eq. (1) shows that E_z and W_r overlap for $\lambda_p/4$ (λ_p is the plasma wavelength) within the donut shaped region. Although with lower accelerating gradients, electrons, and positrons can also accelerate around $r = 0$, for which the overlap between focusing W_r and accelerating E_z fields also occurs for $\lambda_p/4$.

To show that nonlinear donut wakefields can focus and accelerate positrons and electrons, we start by examining a scenario where the laser intensity is marginally above the threshold for the blowout regime. Figure 1 shows simulation results using a laser with $(l,p) = (1,0)$, $a_0 = 3.2$, $w_0 = 7c/\omega_p$, FWHM duration $\tau = 4/\omega_p$, and $\omega_0/\omega_p = 5$. Considering $\lambda_0 = 2\pi c/\omega_0 = 800$ nm this corresponds to a laser with $\simeq$140 mJ, $w_0 = 4.5$ μm, and with $\tau = 10$ fs propagating in a plasma with $n_0 = 6.9\times10^{19}$ cm^{-3}. The simulation uses a moving window propagating at c, with dimensions $20\times62.5\times62.5(c/\omega_p)^3$, divided into $3000\times325\times325$ cells with $2\times1\times1$ particles per cell.

Figure 1(a) shows a self-injected hollow electron bunch. This is in stark contrast with self-injection in the spherical blowout regime, which produces cylindrical beams. In addition to their fundamental importance (they can carry currents exceeding the Alfvén current [23]), hollow bunches can also be relevant for applications. For instance, it has been recently shown that hollow beams could be used as compact collimators for proton bunches in conventional accelerators [21].

Figure 1(b) shows a transverse density slice of the donut wakefield. The darker density ring corresponds to the self-injected bunch. The lighter density rings, inside and outside

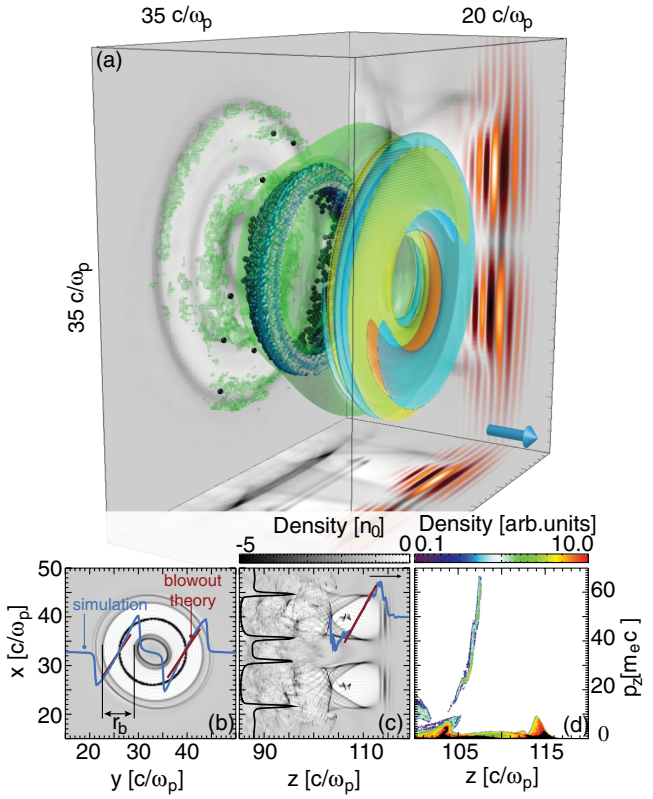

FIG. 1 (color online). OSIRIS simulation result of a hollow self-injected electron bunch. (a) Green-blue colors are plasma density isosurfaces. White-blue spheres are self-injected electrons colored according to their energy (higher energy in white and lower energy in blue). Projections show the plasma density in gray and laser fields in orange-red-brown colors. (b) A transverse slice of the wakefield (laser propagates outside the plane) superimposed by a transverse lineout of plasma focusing fields took in the region where r_b is maximum. Simulation results are in blue and analytical theory in red. (c) A transverse slice of the box. A lineout of the accelerating gradient taken at the center of the bubble is shown in blue and theoretical prediction in red. The solid black line is a lineout of the plasma density at $z = 110\,c/\omega_p$. (d) The plasma phase space, where the hollow electron bunch gains up to 35 MeV. Arrows indicate the direction of laser propagation.

of the darker electron ring, define the donut bubble radially. This structure provides focusing forces that are well described by the analytical scaling for the spherical blowout, $W_r = (r - r_m)/2$, as shown by Fig. 1(b). Hollow bunch electrons then perform betatron oscillations around $r_m \simeq w_0/\sqrt{2}$. Corresponding betatron radiation patterns may lead to the generation of hollow x rays. Longitudinal slices of the donut wakefield [Fig. 1(c)] reveal that the donut wakefield appears as two symmetric bubbles. The accelerating fields at $r = r_m$ [blue line in Fig. 1(c)] also follow the scalings for the spherical blowout, $E_z = \xi/2(m_e c\omega_p^2/e)$ [red line in Fig. 1(c)] [7,8,11].

Since both E_z and W_r are well described by the spherical blowout scaling laws, we can then use them to estimate the

maximum hollow bunch energy gain (ΔE). For the parameters of Fig. 1, $\Delta E \simeq (2/3) m_e c^2 (\omega_0/\omega_p)^2 \sqrt{a_0} \simeq 27$ MeV [11], close to the maximum energies observed in Fig. 1(d). Simulations also showed that the laser is self-guided by the donut blowout during electron acceleration, confirming that energy is efficiently transferred from the laser to the hollow bunch. Although more refined models can be constructed, these results indicate that spherical blowout theory appears to accurately predict key donut wakefield properties in the blowout regime.

Donut bubble transverse wakefields are able to focus and accelerate positrons on axis when the laser radial ponderomotive force is sufficiently intense to push the inner donut electron sheath towards $r = 0$. When this occurs, the electron charge density on axis rises above the background plasma ion density, resulting in a positron focusing field. This condition is met when the donut blowout radius, $r_b \simeq 2\sqrt{a_0}$, matches $r_m = w_0/\sqrt{2}$, i.e., when $a_0 \simeq w_0^2/8$ in our normalized units. We can predict the resulting positron focusing force analytically by recalling that in the blowout, $W_r = E_r - B_\theta$ is electromagnetic in character due to the presence of strong plasma currents. Under the quasistatic approximation and in the Lorentz gauge, $E_r = -\partial_r \phi - \partial_\xi A_r$ and $B_\theta = -\partial_r A_z - \partial_\xi A_r$, where ϕ is the scalar potential, and where A_r and A_z are the radial and longitudinal plasma (slow varying) vector potentials. As a result, $E_r - B_\theta = -\partial_r \phi + \partial_r A_z = -\partial_r(\phi - A_z) = -\partial_r \psi$. The plasma pseudopotential $\psi \equiv \phi - A_z$ hence fully determines W_r, including the contributions from the ion and electron density distribution, and plasma currents [24]. To obtain an expression for ψ, we solve $-\nabla_\perp^2 \psi = 4\pi[n_e(1 - v_\parallel) - 1]$, or, equivalently, $\psi = \ln(r) \int_0^r r' dr' \{n_e(r')[1 - v_z(r')] - 1\} + \int_r^\infty \ln(r') r' \{n_e(r')[1 - v_z(r')] - 1\}$ [24], where $\nabla_\perp^2 = (1/r)\partial_r(r \partial_r \psi)$ is the transverse Laplacian, and where $n_e(1 - v_\parallel) - 1$ is the source term for ψ. We consider a simplified model for $n_e(1 - v_z)$ shown in Fig. 2(a), where

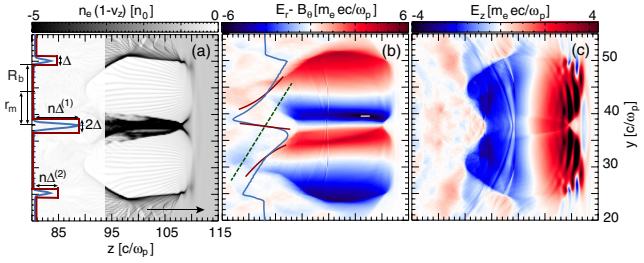

FIG. 2 (color online). OSIRIS simulation result illustrating large amplitude focusing and accelerating fields for positrons in nonlinear regimes. (a) Transverse slice of $n_e(1 - v_z)$. The blue line is a lineout at $z = 115\, c/\omega_p$, and the red line is the simplified model. The quantities R_b, r_m, Δ, $n_\Delta^{(1)}$, and $n_\Delta^{(2)}$ are also indicated. (b) Transverse slice of the transverse focusing force. The blue line is a lineout at $z = 115\, c/\omega_p$, the red line is the theoretical result, and the dashed green line is the theory for the spherical blowout. (c) Transverse slice of the accelerating electric field. The arrow indicates the direction of laser propagation.

the blue line represents the simulation $n_e(1 - v_z)$, and the red line, the simplified model for the calculation. Values for $n_e(1 - v_\parallel)$ at $r = 0$ ($n_\Delta^{(1)}$) and at the bubble wall ($n_\Delta^{(2)}$) can be derived by noticing that $d/d\xi\{\int [n_e(1 - v_\parallel)] d\mathbf{x}_\perp\} = 0$; i.e., $n_e(1 - v_z)$ is conserved in each transverse slice. Assuming further that $\int_0^{R_b/2} [n_e(1 - v_\parallel) - 1] d\mathbf{x}_\perp = \int_{R_b/2}^{R_b + \Delta} [n_e(1 - v_\parallel) - 1] d\mathbf{x}_\perp = 0$, then $n_\Delta^{(1)} = R_b^2/(4\Delta^2)$ and $n_\Delta^{(2)} = [(R_b + \Delta)^2 - (R_b/2)^2]/[(R_b + \Delta)^2 - R_b^2]$, where Δ is the thickness of the electron layers defining the donut blowout [see Fig. 2(a)]. In the relativistic blowout regime $R_b \gg 1$ and $\Delta \ll R_b$ such that

$$\psi = \frac{1}{8}\left[2(R_b^2 - r^2) + R_b^2 \ln\left(\frac{r}{R_b}\right)\right] + \frac{3R_b^2 \alpha}{16}, \qquad (2)$$

for $\Delta < r < R_b$, where $R_b = 2r_b$, and where $\alpha \equiv \Delta/R_b \ll 1$. In addition,

$$\psi = \frac{r^2}{16\alpha^2} + \frac{1}{16}\{-4r^2 + R_b^2[3 + 2\ln(\alpha)]\}, \qquad (3)$$

for $r < \Delta < R_b$. The focusing force is thus

$$W_r = \frac{r}{2} - \frac{R_b^2}{8r}, \qquad (4)$$

for $\Delta < r < R_b$. The first term in Eq. (4) is due to the ion column and the second to the thin on-axis electron layer. In addition,

$$W_r = \frac{r}{2}\left[1 - \frac{1}{4\alpha^2}\right], \qquad (5)$$

for $r < \Delta < R_b$. The first term in Eq. (5) is due to the ion column and the second due to the on-axis electron layer.

Equation (5) reveals that positron focusing fields in donut bubbles can be much higher than the electron focusing fields in spherical bubbles for $r < \Delta$. According to Eq. (5) for $\alpha \ll 1$, the on-axis positron focusing force is $W_r^{e^+} \simeq r/(8\alpha^2)$, whereas for a pure ion spherical bubble $W_r^{e^-} = 1/2$. Hence, for $\alpha \simeq 1/10$, $W_r^{e^+}/W_r^{e^-} \simeq 50$. This may lead to higher frequency x-ray emission by positron bunches in the donut blowout than by electrons in a pure ion spherical bubble [25]. The width of the positron focusing region extends well beyond the width of the on-axis electron layer, lasting from $0 < r < R_b/2$. Moreover, we note that although they may vary due to the dynamics of the inner donut sheath, positron accelerating fields are of the same order of magnitude of those of the spherical blowout. Positron acceleration can therefore occur for the first half of the donut.

We confirmed these findings in 3D PIC simulations. Figure 2 was obtained using identical simulation parameters to Fig. 1, except for the laser a_0. The onset of positron

focusing and acceleration fields on axis for the laser spot size of the simulation shown in Fig. 1 ($w_0 = 7c/\omega_p$) is $a_0 \simeq 6.12$. Figure 2, in which $a_0 = 8 > 6.12$, then confirms that $r_b > w_0$ and that the inner donut bubble electron sheath merges on axis. These parameters correspond to a laser pulse energy of ≃850 mJ. Figure 2(a) shows that the motion of the boundary $R_b(\xi)$ resembles that of a spherical bubble. Figure 2(b) confirms that the donut bubble focusing fields are much higher than those of a spherical bubble, and that in this case $W_r^{e^+}/W_r^{e^-} = 14$. In addition, Fig. 2(b) shows that simulation results for W_r are in good agreement with Eqs. (4) and (5) using $R_b = 11.8$ and $\Delta = 1.5$. Values for R_b and Δ were retrieved directly from Fig. 2(a) at $z = 113.5c/\omega_p$. Figure 2(c) shows very large positron accelerating gradients that overlap with positron focusing wakefields for the first half of the bubble. The peak positron accelerating field in Fig. 2(c) is 15 GV/cm, higher than the peak electron accelerating field at the back of the donut.

We performed simulations to demonstrate the acceleration of a witness positron bunch in the donut wakefields. Figure 3 shows an OSIRIS 3D simulation result using a laser pulse with $(l, p) = (1, 0)$, $w_0 = 6.6c/\omega_p$, $a_0 = 6.8$, $\omega_0/\omega_p = 15$, and $\tau = 3/\omega_p$ (shorter than in the previous simulations to reduce interaction between positrons and laser). We placed a low charge (to avoid beam loading) flattop witness positron bunch with a length of $1c/\omega_p$ and transverse radius $3c/\omega_p$ in regions where initial positron accelerating fields were close to maximum. The witness bunch was injected with $\gamma = 200$ (ensuring that all positrons are trapped) with zero energy spread and zero emittance. These parameters correspond to a laser with $w_0 = 12.6$ μm, $\tau = 19$ fs, and and energy of 2 J propagating in a plasma with $n_0 = 7.7 \times 10^{18}$ cm^{-3}. For this plasma density the witness bunch is 3.84 μm long and 5.76 μm wide. Numerical simulation parameters are identical to those of Fig. 1.

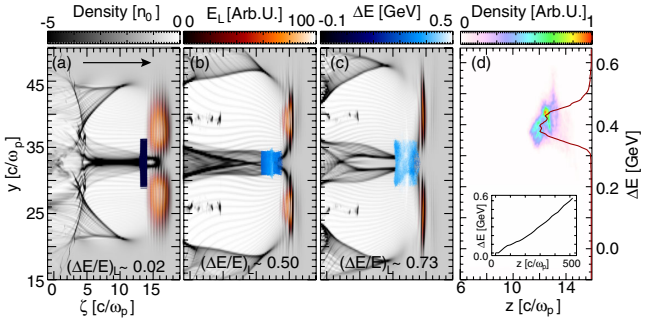

FIG. 3 (color online). OSIRIS simulation result illustrating positron acceleration in the wake driven by a laser pulse with OAM. (a)–(c) Plasma density (gray), laser pulse electric field (orange), and witness positron bunch (blue) colored according to energy gain at $z = 40\,c/\omega_p$ (a), $z = 400\,c/\omega_p$ (b), and $z = 518\,c/\omega_p$ (c). $(\Delta E/E)_L$ indicates the fraction of the depleted laser energy. The arrow indicates the laser propagation direction. (d) Longitudinal phase space and spectrum (red line) of the witness positron bunch at $z = 518\,c/\omega_p$. The inset shows the maximum positron energy as a function of the propagation distance.

Figures 3(a)–3(b) show that the donut bubble can guide the laser pulse. We found that the self-guiding condition for the spherical blowout regime, given by $w_0 \simeq r_b \simeq 2\sqrt{a_0}$, can also be used as an estimate for the self-guided propagation of a donut shaped laser. This can be attributed to the fact that the donut bubble refracting index gradient, which determines the laser dynamics, is identical to that of spherical bubbles (the simulation of Fig. 3 then used $w_0 = 6.6$, close to $2\sqrt{a_0} \simeq 5.2$). Although the on-axis electron sheath oscillates during the laser propagation for these parameters, the plasma wave still provides positron accelerating and focusing fields. Figures 3(a)–3(c) show that the laser drives a stable wakefield ensuring positron acceleration until the laser energy is a small fraction of its initial energy. This is confirmed by the inset of Fig. 3(d), revealing constant acceleration gradients during propagation. The resulting (normalized) average accelerating gradient is $E_{\text{accel}} \simeq 1.5$, much larger than that of the linear regime where $E_{\text{accel}} \ll 1$. After $z = 518c/\omega_p$, the mean positron bunch energy gain is $\Delta E \simeq 400$ MeV [Fig. 3(d)], similar to the mean energy gain of self-injected electrons. Simulations also show that, in agreement with analytical predictions, the transverse donut shaped wakefields focus the positron bunch even though its initial radius is much wider than the on-axis electron sheath.

We note that simulations using hollow electron bunch drivers showed similar initial positron focusing and acceleration regions in nonlinear regimes. These simulations then indicate that our results are determined by the intensity profile of the driver, being independent of its phase content.

In conclusion, we investigated self-injection of hollow electron beams and positron acceleration in donut shaped wakefields driven by Laguerre-Gaussian laser pulses with OAM in the nonlinear regime analytically and with 3D PIC simulations. The onset of positron focusing and accelerating fields occurs when the electron sheath at the inner wall of donut shaped blowout merges on axis. Resulting positron focusing could lead to enhanced betatron x-ray radiation emission regimes in comparison to electrons in the spherical blowout regime. More detailed understanding of externally guided and self-guided regimes will be important to improve the stability of positron and electron acceleration. Other future research directions also include donut wakefield excitation by particle drivers and radially polarized lasers.

This work has been partially supported by FCT (Portugal) through Grant No. EXPL/FIS-PLA/0834/2012. We acknowledge PRACE for access to resources on SuperMUC (Leibniz Research Center). We also acknowledge useful discussions with Professor Luís O. Silva. The authors would like to thank the anonymous referee for the suggestion to include a 3D simulation to demonstrate positron bunch acceleration in the donut blowout regime.

*jorge.vieira@ist.utl.pt
†titomend@ist.utl.pt

[1] T. Tajima and J. M. Dawson, Phys. Rev. Lett. **43**, 267 (1979); R. Bingham, J. T. Mendonça, and P. K. Shukla, Plasma Phys. Controlled Fusion **46**, R1 (2004).
[2] J. T. Mendonça, J. R. Davies, and M. Eloy, Meas. Sci. Technol. **12**, 1801 (2001).
[3] A. Rousse, K. T. Phuoc, R. Shah, A. Pukhov, E. Lefebvre, V. Malka, S. Kiselev, F. Burgy, J.-P. Rousseau, D. Umstadter, and D. Hulin, Phys. Rev. Lett. **93**, 135005 (2004); S. Kneip *et al.*, Nat. Phys. **6**, 980 (2010); G. A. Mourou, T. Tajima, and S. V. Bulanov, Rev. Mod. Phys. **78**, 309 (2006).
[4] R. K. Kirkwood, J. D. Moody, J. Kline, E. Dewald, S. Glenzer, L. Divol, P. Michel, D. Hinkel, R. Berger, E. Williams, J. Milovich, L. Yin, H. Rose, B. MacGowan, O. Landen, M. Rosen, and J. Lindl, Plasma Phys. Controlled Fusion **55**, 103001 (2013).
[5] J. Faure, C. Rechatin, A. Norlin, A. Lifsitz, Y. Glinec, and V. Malka, Nature (London) **444**, 737 (2006); S. P. D. Mangles, C. D. Murphy, Z. Najmudin, A. G. Thomas, J. L. Collier, A. E. Dangor, E. J. Divall, P. Foster, J. G. Gallacher, C. J. Hooker, D. Jaroszynski, A. Langley, W. B. Mori, P. A. Norreys, F. S. Tsung, R. Viskup, B. R. Walton, and K. Krushelnick, Nature (London) **431**, 535 (2004); C. G. R. Geddes, Cs. Toth, J. Tilborg, E. Esarey, C. B. Schroeder, D. Bruhwiler, C. Nieter, J. Cary, and W. P. Leemans, Nature (London) **431**, 538 (2004); W. P. Leemans, B. Nagler, A. J. Gonsalves, Cs. Toth, K. Nakamura, C. G. R. Geddes, E. Esarey, C. B. Schroeder, and S. M. Hooker, Nat. Phys. **2**, 696 (2006).
[6] A. Pukhov and J. Meyer ter Vehn, Appl. Phys. B **74**, 355 (2002).
[7] I. Kostyukov, A. Pukhov, and S. Kiselev, Phys. Plasmas **11**, 5256 (2004).
[8] W. Lu, C. Huang, M. Zhou, W. B. Mori, and T. Katsouleas, Phys. Rev. Lett. **96**, 165002 (2006).
[9] M. Tzoufras, W. Lu, F. S. Tsung, C. Huang, W. B. Mori, T. Katsouleas, J. Vieira, R. A. Fonseca, and L. O. Silva, Phys. Rev. Lett. **101**, 145002 (2008).
[10] S. Kalmykov, S. A. Yi, V. Khudik, and G. Shvets, Phys. Rev. Lett. **103**, 135004 (2009).
[11] W. Lu, M. Tzoufras, C. Joshi, F. S. Tsung, W. B. Mori, J. Vieira, R. A. Fonseca, and L. O. Silva, Phys. Rev. ST Accel. Beams **10**, 061301 (2007).
[12] S. Lee, T. Katsouleas, R. G. Hemker, E. S. Dodd, and W. B. Mori, Phys. Rev. E **64**, 045501(R) (2001).
[13] C. B. Schroeder, C. Benedetti, E. Esarey, and W. P. Leemans, Phys. Plasmas **20**, 123115 (2013).
[14] W. D. Kimura, H. M. Milchberg, P. Muggli, X. Li, and W. B. Mori, Phys. Rev. ST Accel. Beams **14**, 041301 (2011).
[15] E. Esarey and P. Sprangle, IEEE Trans. Plasma Sci. **24**, 252 (1996).
[16] L. Allen, M. W. Beijersbergen, R. J. C. Spreeuw, and J. P. Woerdman, Phys. Rev. A **45**, 8185 (1992).
[17] J. T. Mendonça, B. Thidé, and H. Then, Phys. Rev. Lett. **102**, 185005 (2009).
[18] S. Ali, J. R. Davies, and J. T. Mendonça, Phys. Rev. Lett. **105**, 035001 (2010).
[19] J. T. Mendonça and J. Vieira, Phys. Plasmas **21**, 033107 (2014).
[20] R. A. Fonseca, L. O. Silva, F. S. Tsung, V. K. Decyk, W. Lu, C. Ren, W. B. Mori, S. Deng, S. Lee, T. Katsouleas, and J. C. Adam, in *Lecture Notes in Computer Science*, edited by G. Goos, J. Hartmanis, and J. van Leeuwen (Springer, Berlin, 2002), Vol. 2331, p. 342.
[21] G. Stancari, A. Valishev, G. Annala, G. Kuznetsov, V. Shiltsev, D. A. Still, and L. G. Vorobiev, Phys. Rev. Lett. **107**, 084802 (2011).
[22] E. Cormier-Michel, E. Esarey, C. G. R. Geddes, C. B. Schroeder, K. Paul, P. J. Mullowney, J. R. Cary, and W. P. Leemans, Phys. Rev. ST Accel. Beams **14**, 031303 (2011).
[23] J. R. Davies, Phys. Rev. E **68**, 037501 (2003).
[24] W. Lu, MsC thesis, University of California Los Angeles, 2004.
[25] I. Kostyukov, S. Kiselev, and A. Pukhov, Phys. Plasmas **10**, 4818 (2003).